Structure and thermal stability of Fe : Al_2O_3 nanocomposite films

2002 J. Phys. D: Appl. Phys. 35 916

(http://iopscience.iop.org/0022-3727/35/9/313)

INSTITUTE OF PHYSICS PUBLISHING JOURNAL OF PHYSICS D: APPLIED PHYSICS

J. Phys. D: Appl. Phys. **35** (2002) 916–922 PII: S0022-3727(02)30280-8

Structure and thermal stability of Fe : Al_2O_3 nanocomposite films

G T Fei[1], J P Barnes[1], A K Petford-Long[1,3], R C Doole[1], R Serna[2] and J Gonzalo[2]

[1] Department of Materials, University of Oxford, Parks Road, Oxford OX1 3PH, UK
[2] Instituto de Optica, CSIC, Serrano 121, 28006 Madrid, Spain

E-mail: amanda.petford-long@materials.ox.ac.uk

Received 31 October 2001
Published 16 April 2002
Online at stacks.iop.org/JPhysD/35/916

Abstract

Nanocomposite films consisting of Fe nanocrystals (NCs) embedded in an amorphous Al_2O_3 matrix have been fabricated by alternate pulsed laser deposition in vacuum. The size, shape and distribution of the Fe NCs have been analysed by high resolution electron microscopy. The thermal stability of the films has been studied by *in situ* annealing in the electron microscope, and the chemical state of the Fe has been investigated by electron energy loss spectroscopy. The nucleation and growth of the Fe NCs has been studied as a function of the number of pulses. Nucleation is homogenous over the surface of the Al_2O_3 at the beginning of deposition. The distribution of the NCs is uniform and their in-plane shape can be approximated by ellipses for a small number of pulses on the Fe target. As the Fe content increases some adjacent NCs coalesce resulting in a sudden increase in dimensions and in-plane aspect ratio. Isothermal annealing treatments for up to 160 min show that the Fe NCs are stable up to 400°C, with morphological changes occurring at higher temperatures. The as-prepared Fe NCs were found to be α-Fe and no changes of oxidation state of Fe were observed after annealing.

1. Introduction

Nanocomposite materials, such as nanocrystals (NCs) embedded in a continuous matrix, have attracted considerable research effort in recent years both because of their potential technological applications and because of their relevance to the study of basic physical properties in the mesoscopic size range [1–3]. On decreasing the dimensions of a material to the nanometre scale, many new effects appear, such as quantum size effects, which can result in new physical properties so that nanostructured materials can show novel optical, electrical, magnetic and catalytic properties that are different from those of bulk materials [3]. For example, the magnetic properties of Fe NCs dispersed in an insulating matrix are different from those of bulk Fe [4, 10] with the coercivities of the NCs being two orders of magnitude higher than that of pure Fe [10] and the magnetocrystalline anisotropy being higher than that of bulk Fe [6, 11]. Many properties are closely related to the size, shape and distribution of the NCs [4–8]. The coercivity of the Fe NCs is inversely proportional to their separation [8], and the NC shape can give rise to interesting anisotropic properties [7]. The electrical conductivity is also related to NC size and separation [12]. Nevertheless, the study of NC formation, and characterization of their size, shape and growth mechanisms has been very limited [9].

Many techniques can be employed to fabricate nanocomposite films, such as sol–gel [13], sputtering [4, 10] and ion implantation [14]. Pulsed laser deposition (PLD) is a more recently developed thin film technique that has been used to prepare high quality nanocomposite films for optical applications [9, 15, 16]. The use of alternate PLD from separate matrix and metal targets has proved to be advantageous. In this way, the properties of the matrix and metal NCs can be controlled independently, and thus it is possible to control the size and shape of the NCs as has been shown for Cu [17, 18]. Recently, we have shown that PLD Fe NCs can show special magnetic behaviour due to their reduced dimensions, and a high temperature superparamagnetic regime has been identified [19]. In this paper, we discuss the growth mechanism of the Fe NCs embedded in an amorphous Al_2O_3 matrix. Our aim is to understand

[3] Author to whom correspondence should be addressed.

the relationship between deposition and growth processes, and the size, shape and distribution of the Fe NCs. This knowledge will enable nanocomposite films with suitable properties to be produced by PLD. Moreover, we address two other important aspects related to the applicability of these films, their thermal stability under annealing treatments and the Fe oxidation state, as it is well known that the oxidation state of the metal strongly affects its properties [19–21].

2. Experimental details

The films were deposited in vacuum ($<10^{-6}$ mbar) using an ArF excimer laser ($\lambda = 193$ nm, $\tau = 20$ ns full width at half maximum, 5 Hz repetition rate) to ablate high purity targets of Al_2O_3 and Fe alternately with an energy density of ~ 2 J cm^{-2}. The targets were placed on a computer-controlled holder and rotated during ablation to prevent crater formation. The substrates, which were located along the normal to the target at a distance of 32 mm, were carbon-coated mica and were kept at room temperature during deposition. The deposition sequence involved 800 pulses on Al_2O_3 first, and then a chosen number of pulses on the Fe target, followed by a further 800 pulses on the Al_2O_3 again in order to obtain a sandwich structure of $Al_2O_3/Fe/Al_2O_3$ on the substrate. This structure prevented the Fe NCs being exposed to air, whilst allowing analysis of a single layer of Fe NCs, since in the case of films containing several Fe layers the overlap of NCs in the plan-view images prevents their size and separation from being correctly determined. From previous experiments it has been found that the number of pulses to obtain well separated Fe NCs, i.e. before percolation, has to be under 250 pulses on the Fe target. Thus, for this work three samples with 100, 150 or 200 pulses on the Fe target were prepared. They are named Fe100, Fe150, and Fe200, respectively.

HRTEM specimens were prepared by floating the films off the mica in distilled water and picking them up on Au TEM grids. The films were analysed in plan-view using a JEOL 4000EX HRTEM operated at 400 kV (point-to-point resolution 0.16 nm). In each case care was taken to prepare HRTEM specimens from the same region of the substrate, since it is known that the NC density produced by the laser deposition process decreases with distance from the centre of the substrate [17, 22].

The *in situ* thermal annealing experiments were performed in another JEOL 4000EX TEM operated at 400 kV (point-to-point resolution 1 nm). Samples were annealed isothermally at 200°C, 400°C, 600°C and 800°C, respectively. The temperature was continuously increased to the desired temperature over 3 min and then kept at this temperature for 2 h 40 min. Images can only be recorded after about 30 min from the start of heating because of drift of the sample. After annealing the samples were observed in the 4000EX HRTEM. A JEOL 3000FEG TEM was used to obtain EELS spectra and Fe composition maps using the Fe $L_{2,3}$ edge. The beam was focused to give a spatial resolution of ~ 1 nm. Care was taken during TEM analysis to use conditions that would not result in electron-beam induced crystallization of the Al_2O_3 matrix.

In order to determine the three-dimensional shape of the Fe NCs, cross-section samples were observed, which were prepared using a focused ion beam (FIB) system (FEI 200TEM). For this experiment, multilayer films were prepared on Si substrates under similar conditions to those used for the sandwich films, i.e. same number of pulses on the Fe target. In this case, five Fe deposits, instead of one, were alternated with the deposition of the Al_2O_3 layers.

Quantitative statistical analysis of the NC morphology was obtained by manually outlining the NCs in the HRTEM image to form a binary image which can be easily analysed using the Gatan Digital Micrograph software.

3. Results and discussion

3.1. Growth process

Figure 1 shows HRTEM images of the three Fe : Al_2O_3 nanocomposite films with (a) 100, (b) 150 and (c) 200 pulses on the Fe target, respectively. The NCs show up as dark features in the image superimposed on a background of random contrast. The NCs are relatively hard to see, partly because they are capped above and below by 10 nm thick layers of Al_2O_3 matrix, and the plan-view images are a projection through two Al_2O_3 layers and only one layer of Fe NCs. The binary images of the same area shown in the HRTEM image for each specimen are also included in figure 1. The morphology and spatial distribution of the NCs then becomes clearly visible. For Fe100 the NCs have rounded edges and are elliptical with an in-plane aspect ratio close to 1. The surface distribution of the NCs is fairly homogeneous. For sample Fe150, although the majority of the NCs are still elliptical in shape, a few NCs

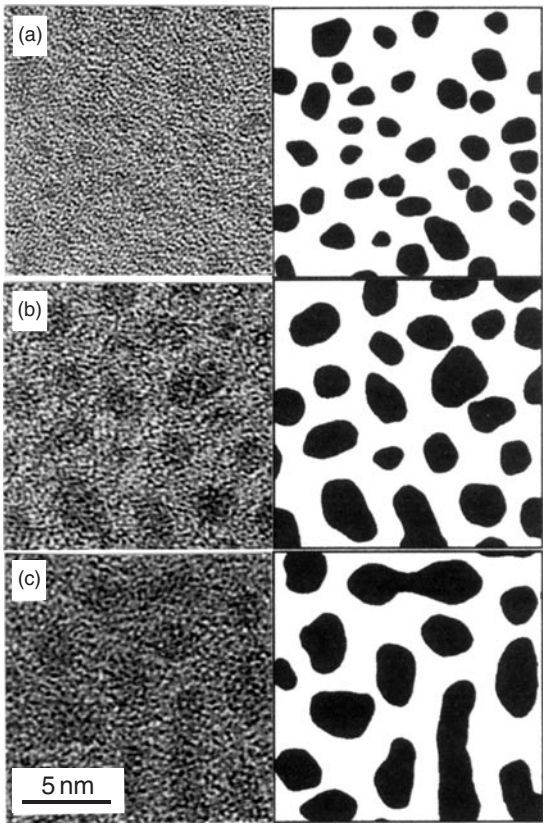

Figure 1. HRTEM and binary images of Fe NCs dispersed in an amorphous Al_2O_3 matrix. Note that the HRTEM images and binary images show the same area. (*a*) Fe100; (*b*) Fe150; (*c*) Fe200.

now have an aspect ratio greater than 2 : 1 and are often bent along the length axis. Part of one such NC can be seen at the bottom of the image. The average size of the NCs has clearly increased with respect to those of Fe100. When the number of laser pulses on the Fe increases to 200, the number of high aspect ratio NCs increases and several of these can be clearly seen in the binary image. The majority, however, remain elliptical with an aspect ratio smaller than 2 : 1. There is no preferred orientation for the elongated NCs.

Figure 2 shows the in-plane surface area distribution of the NCs for the three films. The distribution is very narrow for Fe100, and is already very much broadened for Fe150. As the number of pulses on the Fe increases so the surface area of individual NCs increases. Though the maximum in the distribution is located at the same position for Fe150 and for Fe200, the percentage of NCs with a large area is higher for Fe200 than for Fe150 resulting in a shift of the distribution for Fe200 relative to that for Fe150. The average NC areas for Fe100, Fe150 and Fe200 are 2.4, 5.2 and 8.1 nm^2, respectively.

In order to study the shape of the NCs their short axis (width) and long axis (length) have been measured. As expected, the mean width and length increase with the increase of Fe content. The average lengths/widths are 2.1/1.6, 3.2/2.2 and 4.2/2.7 nm for Fe100, Fe150 and Fe200, respectively. In figure 3(*a*) the NC length distribution is shown. It is seen that the distribution becomes broader as the Fe content is increased, and it is noticeable that for Fe200 there are some very long NCs with sizes up to 20 nm, when the mean value is only 4.2 nm. This shows that NCs with very different dimensions are co-existing in this film. Figure 3(*b*) shows the distribution of NC aspect ratios (length/width) for the three films. The maximum of the distribution is located at a value of 1.3 for all three films: this means that the length is only 25% larger than the width implying that the majority of the NCs have quasi-circular in-plane shape. For Fe100 the distribution is narrow with a single maximum. For Fe150 the distribution shows an additional shoulder at about 2.0, showing that there are about 9% of NCs that are clearly elongated with the length at least twice the width. For Fe200 the distribution broadens significantly and there are NCs with aspect ratios as large as 3.7. Such NCs can be observed in figure 1(*c*).

In order to determine the centre-to-centre separation, the closest neighbour was first determined, and the distance to it measured. Then the NCs within a distance of 1.4 times this distance were selected for calculating the NC average separation. Figure 4 shows the centre-to-centre separation distribution for the NCs. As the amount of Fe increases so does the size of the NCs, and their centre-to-centre distance increases, the mean value being only slightly larger than that of the average length of the NCs (see figure 3(*a*)). As more Fe arrives to the surface the NCs grow and those that are very close tend to become closer and eventually coalesce forming a single NC. Note that for samples Fe150 and Fe200 the number of NCs separated by less than 2 nm is negligible.

Figure 5 shows cross-section HREM images for (a) Fe150 and (b) Fe200. Two dark layers are visible in each micrograph corresponding to two of the five Fe deposits, and they are separated by the low contrast Al_2O_3 layer. In this figure, the lattice fringes visible in some regions of the Al_2O_3 matrix can be identified as crystalline Al_2O_3 caused by electron beam radiation although conditions were used so as to try to minimize this effect. As we are looking through a projection, images of different Fe NCs are overlapped and it is difficult to see the independent shapes. Nevertheless the average height of the Fe NCs can be measured. For Fe150 the average height is 1.3 nm, and for Fe200 is around 2.5 nm. This means that the dimension of the NCs normal to the film plane tends to be smaller than the in-plane dimensions.

During the laser ablation deposition process, the atomic species coming from the target carry high energy. In our system, for laser energy densities of a few J cm^{-2} it has been

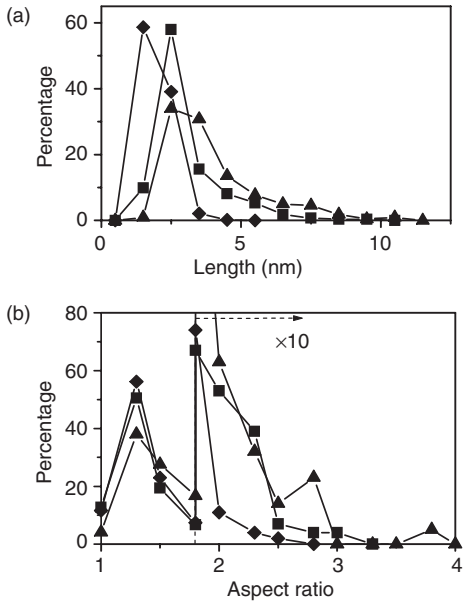

Figure 3. The (*a*) length and (*b*) aspect ratio distributions for the NCs: ♦: Fe100; ■: Fe150; ▲: Fe200.

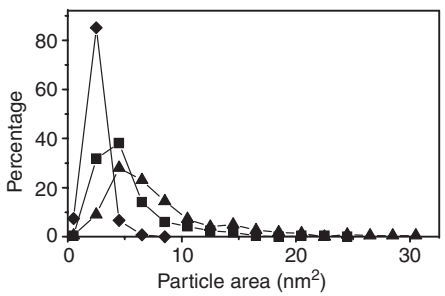

Figure 2. The area distribution of the NCs: ♦: Fe100; ■: Fe150; ▲: Fe200.

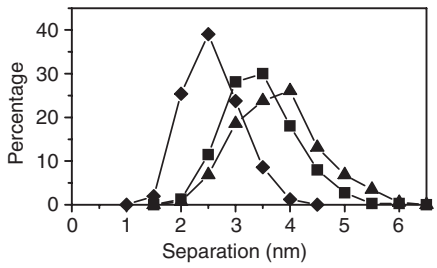

Figure 4. The centre-to-centre separation distribution of the NCs: ♦: Fe100; ■: Fe150; ▲: Fe200.

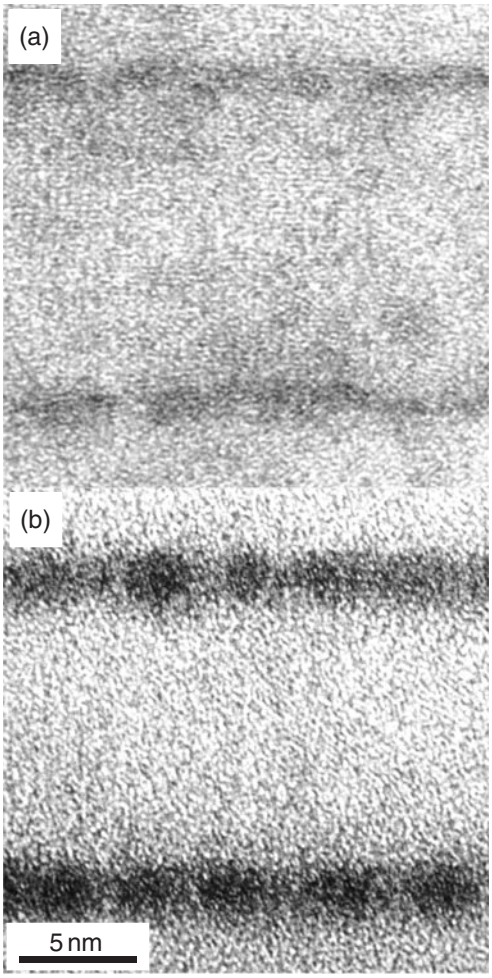

Figure 5. Cross-section HRTEM images of (*a*) Fe150 and (*b*) Fe200.

found that the velocities of the ablated species are typically around 1×10^4 m s^{-1} [23]. Taking into account the mass of Fe (55.85 amu), the estimated kinetic energy of the species arriving at the substrate is about 50 eV. When an Fe atom arrives at the surface of the substrate, it can be adsorbed onto the surface, it can diffuse across the surface, or it can desorb from the substrate surface. These processes allow the species to transfer their energy to the substrate and cool down. Since the physical adsorption energy is very low (usually around 0.5 eV [24]), diffusion of the Fe atoms on the surface of the Al_2O_3 is expected to be a common phenomenon. This surface diffusion will continue until the species do not have enough energy. When two or more Fe atoms meet following surface diffusion, they can combine to form a cluster. The fact that figure 1(*a*) shows a homogenous surface distribution of NCs suggests that there are no, or few, surface defects with deep energy wells present on the pre-deposited amorphous Al_2O_3 film surface, so that there is a homogenous distribution of nuclei over the surface. If the number of atoms in a cluster reaches the critical nucleus size, the cluster becomes stable and further growth depends on the capture of more diffusing Fe species. The location on the Al_2O_3 surface at which the Fe species arrive is random, as is the diffusion direction on the surface. This means that the growth of the nuclei is homogenous, the shape of the NCs is near circular, and the distributions of NC area, length and width are narrow, as can be seen from the plots in figures 2 and 3 for Fe100 (♦ symbols). The mobility of the nuclei is much lower than that of the atomic species, and with increasing size, the mobility of the NCs decreases further [25].

With increasing number of pulses on the Fe target, the NC size increases, as can be seen from the images in figures 1(*b*) and (*c*) and from the plots in figures 2–4. Two growth stages can be distinguished, which lead to the different observed NC shapes. Initially, the NCs grow by coarsening with the disappearance of some of the very small NCs at the expense of others. This leads to an increase in NC size but without a change in the in-plane aspect ratio. With the disappearance of some very small NCs, the centre-to-centre separation increases. This is the main growth process that takes place between samples Fe100 and Fe150, resulting in similar aspect ratio plots, but an increase in NC average size and separation. Further growth then occurs by the coalescence of adjacent NCs, which leads to the formation of elongated NCs and an increase in NC aspect ratio. The beginning of this growth stage can be already seen for sample Fe150 with the formation of the shoulder at a value of around 2 in the aspect ratio (figure 3(*b*)), which indicates that more elongated NCs are being formed from coalescence of NCs. As the amount of Fe arriving at the substrate surface increases the number of coalescence events increases, and now coalescence of more than two NCs can be observed leading to the formation of very long 'rods' (see figure 1(*c*)). Thus, for sample Fe200 there are both NCs increasing in size by coarsening, with aspect ratio which is the same as for the other two samples, and also there is the coalescence of two or more NCs which gives rise to NCs with aspect ratio higher than 2.

Therefore, in order to obtain a narrow size and shape distribution and homogenous surface distribution, coalescence should be avoided, so the number of pulses on the Fe target should not exceed the threshold value, between 100 and 150 under the conditions used here.

From the analysis of the TEM results, it is shown that PLD of Fe on Al_2O_3 results in growth via the formation of three-dimensional islands, i.e. it is of Volmer–Weber type. In fact this is the growth mode found for many metals deposited on oxides by other techniques [26, 27]. Thus, it seems that the growth mode is strongly influenced by the metal–surface interaction. In our case, the surface free energies of liquid Fe ($\gamma_{v/m}$) and solid Al_2O_3 ($\gamma_{v/ox}$), and the adhesion energy of liquid Fe on Al_2O_3 (E_{adh}), are 1787, 650–925 and 1205 mJ m^{-2}, respectively [26, 28]. It is assumed that the solid metal has a similar interfacial energy on the oxide as the liquid metal, and that $\gamma_{v/m}$ is about 7% larger for the solid than the liquid metal [29], so that $\gamma_{v/m}$ for solid Fe is 1912 mJ m^{-2}. The Fe : Al_2O_3 interfacial free energy $\gamma_{m/ox}$ is 1357–1632 mJ m^{-2}, which is deduced from the equation

$$E_{adh} = \gamma_{v/ox} + \gamma_{v/m} - \gamma_{m/ox}$$

The contact angle θ can be calculated from

$$\cos\theta = \frac{\gamma_{v/ox} - \gamma_{m/ox}}{\gamma_{v/m}} \qquad (30)$$

giving $\theta = 112^\circ$. This contact angle value means that Fe cannot wet Al_2O_3 and so it is more favourable to form a three-dimensional NC on Al_2O_3 rather than a continuous layer.

A comparison of the $Fe : Al_2O_3$ nanocomposite system and other metal systems such as $Ag : Al_2O_3$ [22] and $Cu : Al_2O_3$ [17], grown using the same deposition system and conditions as for the $Fe : Al_2O_3$ system, shows that the initial density of nucleation sites for the Fe is much higher. For example, when the areal density is 39% (Fe150), the number density of Fe NCs is $77.9 \times 10^3\ \mu m^{-2}$, while for Ag at an areal density of 40%, the number density of NCs is $6.8 \times 10^3\ \mu m^{-2}$, and for Cu NCs the number density is $13.3 \times 10^3\ \mu m^{-2}$ at an areal density of 36.4%. This fact suggests that the Fe atomic species have a much lower mobility over the Al_2O_3 surface.

3.2. Thermal stability

The nanocomposite films were annealed *in situ* in the TEM for 2 h 40 min at different temperatures. Figure 6 shows HREM images of Fe200 taken before annealing and after annealing, and subsequent cooling at 600˚C and 800˚C. The corresponding images for the annealing at 200˚C and 400˚C are not shown since no changes could be seen. The image for the as-grown sample shows the typical elongated NCs that have been described for this sample in figure 1(*c*). After annealing at 600˚C it can be seen that the Fe NCs have circular in-plane shapes and are somewhat bigger. After annealing at 800˚C the NCs are faceted and have a hexagonal shape. Around them there is a dark halo that may be the result of a high residual Fe atomic density. The NCs now show a high contrast, compared to the as-grown sample, and are easier to observe against the lighter background. This could be due to an increase of the NCs dimensions and/or to structural reorientation of the NCs thus increasing the diffraction contrast. At this stage, the Al_2O_3 has also crystallized and in some areas lattice fringes can be observed.

In order to follow up the changes during the 800˚C annealing, TEM images were taken during the process. Figure 7 shows selected images taken for film Fe200 during the annealing process. Note that the magnification is low in order to observe the evolution over a large area and as a consequence, the NCs are not seen in the first image of the series, which is of the as-deposited film (figure 7(*a*)). At 800˚C changes appear at the very early stages of the annealing process. After about 11 min (image not shown), dark spots with a homogenous distribution begin to appear. Their shape is approximately circular with roughly uniform size, and as a function of time they tend to grow. After about 36 min (figure 7(*b*)) some of the NCs begin to show hexagonal shapes, after 1 h 15 min (figure 7(*c*)) most of the NCs are hexagonal. Although the change in shape is not clear in figure 7 because of the low magnification at which the experiment was followed, the facetted hexagonal shape of the NCs can be seen clearly in figure 6(*c*). Up to the end of the annealing (2 h 40 min) no significant changes occur (see figure 7(*d*)), apart from a ripening of particle size. Regarding the background contrast, it should be noticed that in figure 7(*b*) large areas with slightly dark contrast appear. They have been identified as areas in which the initially amorphous Al_2O_3 matrix has crystallized to form γ-Al_2O_3 [22]. Figure 8 shows an HREM image of one of the Fe NCs after annealing and subsequent cooling, with the corresponding microdiffraction pattern. The lattice fringes are clearly seen over the NC and the microdiffraction pattern shows that it is a single crystal with bcc structure. The facets of the NCs are {110} type planes.

The most noteworthy features observed during the annealing process are: first an increase in contrast of the Fe NCs, as has already been discussed, and second, a gradual increase in their size. This increase in size is achieved at the cost of the disappearance of the smaller NCs and any atomic

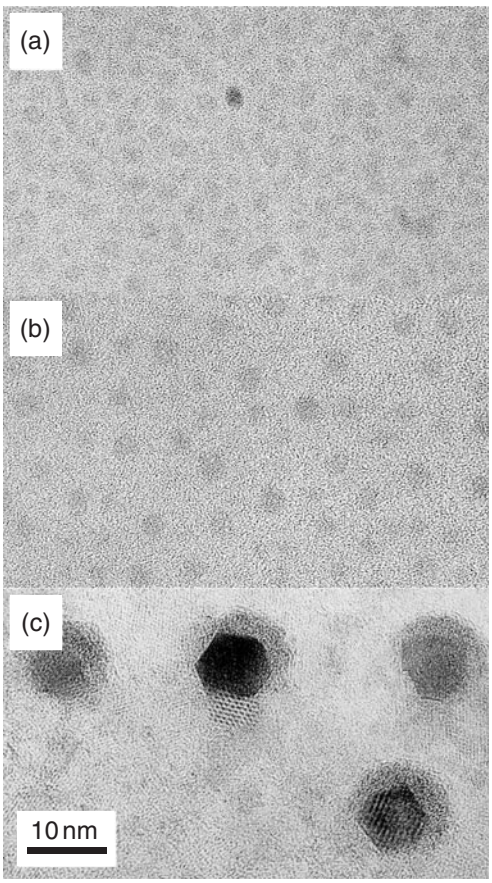

Figure 6. HRTEM image of sample Fe200 (*a*) before annealing and after annealing (and subsequent cooling) at (*b*) 600˚C and (*c*) 800˚C for 2 h 40 min.

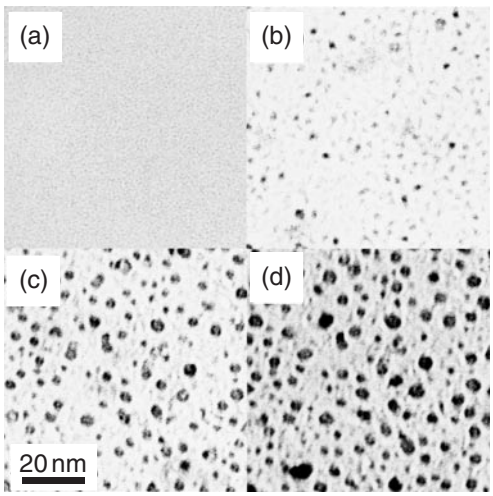

Figure 7. *In situ* TEM images of sample Fe200 taken during annealing at 800˚C, (*a*) before annealing; (*b*) after 36 min; (*c*) after 1 h 47 min; (*d*) after 2 h 40 min.

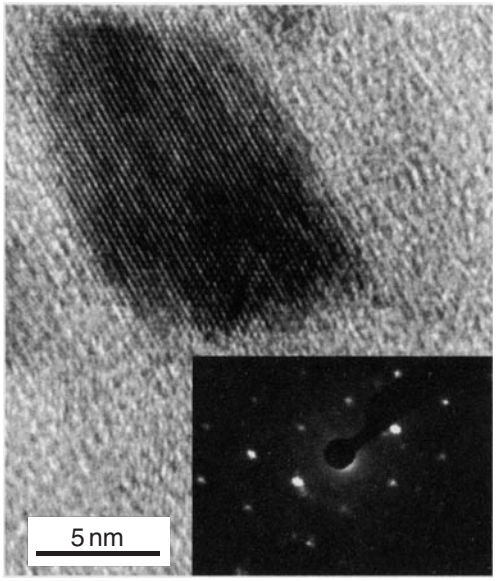

Figure 8. HRTEM image and microdiffraction pattern of sample Fe200 after annealing at 800˚C for 2 h 40 min.

Fe and very small Fe clusters, not necessarily crystalline, that may have formed upon deposition. It should be pointed out that Fe particles with characteristic sizes smaller than 2 nm are very difficult to observe when embedded in an Al_2O_3 matrix. The diffusion process of Fe in amorphous Al_2O_3 has been characterized in Fe/Al_2O_3 multilayers and it is found to be strongly thermally activated [31]. When annealing at low temperature, such as 200˚C and 400˚C, not enough diffusion can occur, so no observable change happens. Upon increasing the temperature to 600˚C, the diffusion rates are high enough to lead to average diffusion distances of the order of 8 nm over 2 h. This is of the order of magnitude of the separation between Fe NCs, and therefore is sufficient to allow the coarsening in size of the NCs that we have observed. At 800˚C the average diffusion distance is of the order of 70 nm after 2 h, which could explain the extensive coarsening, and reorganization of the NCs observed. In addition to the Fe diffusion that occurs when the film is kept at high temperature for a long time, the NCs have enough time to change their shape and faceting occurs. Firstly, they become circular to lower their surface energy, and then they form low energy surface facets in order to decrease the energy further. The Fe has a bcc structure and the (110) plane is the closest packed plane, which is why the facets are {110} planes. It is suggested that the intermediate contrast areas around the hexagonal NCs correspond to regions of Al_2O_3 containing a high Fe density, which form during the Fe diffusion process. It is suggested that if the sample were kept at high temperature for a sufficient time, all of the NCs would become hexagonal in shape with {110} facets. Note that the random-shaped dark regions extending across the Al_2O_3 matrix are regions of the matrix that have crystallized.

3.3. Chemical state

In order to check the chemical state of the NCs before and after annealing, a JEOL 3000FEG TEM was used to obtain composition map images and EELS spectra. Figure 9 shows (*a*) a bright field TEM image and (*b*) an Fe composition image.

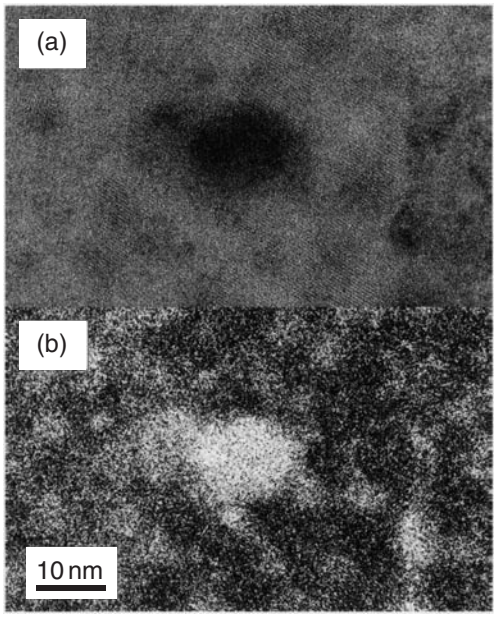

Figure 9. HRTEM image (*a*) and Fe jump ratio image (*b*) of sample Fe200 taken after annealing at 800˚C for 2 h 40 min.

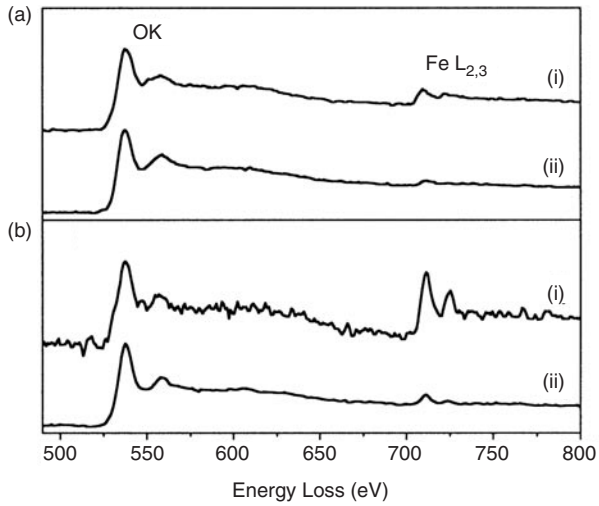

Figure 10. EELS spectra for sample Fe200 (*a*) before, and (*b*) after annealing at 800˚C for 2 h 40 min. In each case, spectrum (i) was recorded on a NC, and spectrum (ii) on the matrix.

By comparing these two images, it can be seen that the dark features that are the NCs in (*a*) correspond to the light features that are the position of the Fe atoms in (*b*), therefore confirming that all of the NCs observed in the TEM images consist of Fe. In order to determine the chemical state of the Fe NCs, EELS spectra were recorded from the NCs and matrix before and after annealing. Figure 10(*a*) shows part of the EELS spectra with the oxygen K edge and Fe $L_{2,3}$ edges before annealing. Spectrum (i) was recorded on a NC and spectrum (ii) was recorded on the matrix. In this case, in order to overcome the fact that the NCs are difficult to observe, several spectra were collected from different areas of the sample and were carefully compared. Figure 10(*b*) shows the EELS spectra obtained after annealing, (i) on a NC and (ii) on the matrix. Comparing the Fe $L_{2,3}$ peaks before and after annealing with

those in the standard spectra for FeO, Fe_3O_4, α-Fe_2O_3 and γ-Fe_2O_3 [32, 34], it can be found that the peak ratio in our spectra is quite different from that in Fe_2O_3. It is found that the Fe $L_{2,3}$ edge is very similar to that for pure Fe obtained from an $Fe_{73.5}Cu_1Mo_3Si_{13.5}B_9$ alloy [35] and an Fe-16Cr-17Ni alloy [36]. The oxygen K edge corresponds to that of the Al_2O_3[37], as it should be expected since the amount of Al oxide is very large compared to the Fe oxide that can be potentially formed. These results suggest that the majority of the Fe forming the NCs remains metallic which is probably a result of the affinity of Al to oxygen being larger than that of Fe to oxygen, as it has been shown in multilayer structures [33]. However, the EELS technique used was not sensitive enough to detect the presence of a thin Fe oxide layer on the surface of the NCs so this possibility cannot be ruled out, especially as the Fe NCs are coated in an oxide matrix. Likewise, the composition of the area of intermediate contrast around the hexagonal NCs formed during annealing at 800˚C could not be successfully determined by EELS. The EELS data presented here show that even when the dimensions of the Fe decrease to the nanoscale, it is still difficult to oxidize Fe NCs, even at high temperature. Thus, high quality nanocomposite films formed by metallic Fe embedded in Al_2O_3 can be produced.

4. Conclusion

Alternate PLD in vacuum has been used to fabricate nanocomposites consisting of Fe NCs embedded in an amorphous Al_2O_3 matrix. The Fe nuclei form homogeneously on the surface of the Al_2O_3 at the beginning of deposition. The surface distribution of NCs is homogenous and their in-plane shape is circular or slightly elliptical with a small number of pulses on the Fe target. When the number of pulses on the Fe target increases, then coarsening and coalescence of the NCs occur. The size and distribution of the NCs can be easily controlled by adjusting the number of pulses on Fe. The NCs are stable up to 400˚C for a long time. Annealing at 600˚C made the NC shape become more circular and the size increased. Further increasing the temperature to 800˚C resulted in the NCs becoming facetted and hexagonal in shape. The hexagon is composed of $\{110\}$ plane facets. EELS showed that the Fe NCs remained un-oxidized even after annealing.

Acknowledgments

This work was partially supported by CICYT (Spain) under TIC99-0866 project. We are grateful to Dr R M Langford for help preparing the cross-section samples and to Dr C J D Hetherington for help using the 3000F TEM. G T F is grateful to the Chinese Academy of Sciences for support and J P B is grateful to the EPSRC for support. Travelling has been supported through the Acción Integrada Hispano-Británica scheme (HB-98-0182).

References

[1] Gleiter H 1995 *Nanostruct. Mater.* **6** 3
[2] Halperin W P 1986 *Rev. Mod. Phys.* **58** 533
[3] Lu K 1996 *Mater. Sci. Eng. R* **16** 161
[4] Liou S H and Chien C L 1988 *Appl. Phys. Lett.* **52** 512
[5] Serna R, Missana T, Afonso C N, Ballesteros J M, Petford-Long A K and Doole R C 1998 *Appl. Phys.* A **66** 43
[6] Hosono H, Abe Y and Matsunami N 1992 *Appl. Phys. Lett.* **69** 2613
[7] Takakuwa M, Baba K and Miyagi M 1996 *Opt. Lett.* **21** 1195
[8] Bian B, Hirotsu Y and Makino A 1997 *NanoStruct. Mater.* **8** 1057
[9] Serna R, Afonso C N, Ballesteros J M, Naudon A, Babonneau D and Petford-Long A K 1999 *Appl. Surf. Sci.* **138/139** 1
[10] Xiao G and Chien C L 1987 *Appl. Phys. Lett.* **51** 1280
[11] Roy S, Roy B and Chakravorty D 1996 *J. Appl. Phys.* **79** 1642
[12] Abeles B, Sheng P, Coutts M D and Arie Y 1975 *Adv. Phys.* **24** 407
[13] De G, Tapfer L, Catalano M, Battaglin G, Caccavale F, Gonella F, Mazzoldi D and Haglund R F Jr 1996 *Appl. Phys. Lett.* **68** 3820
[14] Magruder R H III, Haglund R F Jr, Yang L, Wittig J E and Zuhr R A 1994 *J. Appl. Phys.* **76** 708
[15] Ballesteros J M, Serna R, Solis J, Afonso C N, Petford-Long A K, Osborne D N and Haglund R F Jr 1997 *Appl. Phys. Lett.* **71** 2445
[16] Wilson N, Petford-Long A K, Doole R C, Serna R and Afonso C N 1998 *J. Appl. Phys.* **84** 5283
[17] Serna R, Gonzalo J, Suárez-García A, Afonso C N, Barnes J P, Petford-Long A K, Doole R C and Hole D 2001 *J. Microscopy* **201** 250
[18] Afonso C N, Gonzalo J, Serna R, De Sande J C G, Ricolleau C, Grigis C, Gandais M, Hole D E and Townsend P D 1999 *Appl. Phys.* A **69** S201
[19] Dempsey N M, Ranno L, Givord D, Gonzalo J, Serna R, Fei G T, Petford-Long A K, Doole R C and Hole D E 2001 *J. Appl. Phys.* **90** 6268
[20] Prados C, Multigner M, Hernando A, Sánchez J C, Fernández A, Conde C F and Conde A 1999 *J. Appl. Phys.* **85** 6118
[21] Jonsson B J, Turkki T, Strom V, E-Shall M S and Rao K V 1996 *J. Appl. Phys.* **79** 5063
[22] Barnes J P 2000 *Part II Thesis* University of Oxford
[23] Gonzalo J, Vega F and Afonso C N 1995 *J. Appl. Phys.* **77** 6588
[24] Smith D L 1995 *Thin-film Deposition: Principle and Practice* (New York: McGraw-Hill) p 123
[25] Chang C M, Wei C M and Chen S P 2000 *Phys. Rev. Lett.* **85** 1044
[26] Campbell C T 1997 *Surf. Sci. Reports* **27** 1
[27] Colaianni M L, Chen P J and Yates J T Jr 1990 *Surf. Sci.* **238** 13
[28] Chatain D, Rivollet I and Eustathopoulos N 1986 *J. Chim. Phys.* **83** 561
[29] Overbury S H, Bertrand P A and Somorjai G A 1975 *Chem. Rev.* **75** 547
[30] Adamson A W 1990 *Physical Chemistry of Surfaces* (New York: Wiley)
[31] Ernst K H, Ludviksson A, Zhang R, Yoshihara J and Campbell C T 1993 *Phys. Rev.* B **47** 13782
[32] Ahn C C and Krivanek O L EELS atlas: a reference guide of electron energy loss spectra covering all stable elements (Gatan)
[33] Sousa R C, Sun J J, Soares V, Freitas P P, Kling A, Da Silva M F and Soares J C 1998 *Appl. Phys. Lett.* **73** 3288
[34] Colliex C, Manoubi T and Ortiz C 1991 *Phys. Rev.* B **44** 11402
[35] Yang G Y and Zhu J 2000 *J. Magn. Magn. Mater.* **220** 65
[36] Ono K, Arakawa K, Oohashi M, Kurata H, Hojou K and Yoshida N 2000 *J. Nucl. Mater.* **283–287** 210
[37] de la Cruz W and Cota Ariaza L *Phys. Stat. Sol.* B **220** 569
[38] Lenoble O, Bobo J F, Fischer H, Bauer Ph, Ravet M F and Piecuch M 1995 *J. Mater. Res* **10** 3062